Some Aspects of the Characteristics of Monsoon Disturbances Using a Combined Barotropic–Baroclinic Model

N. R. Parija and *S. K. Dash*

Centre for Atmospheric Sciences, Indian Institute of Technology, Hauz Khas, New Delhi–110016, India

Received December 19, 1994; revised March 24, 1995

ABSTRACT

A standing Rossby wave of wavelength 30° longitude with a finite amplitude along the meridional direction is superimposed on the zonal mean component of the monsoon flow and the stability of such a flow is examined by a quasi–geostrophic barotropic, as well as by a quasi–geostrophic combined barotropic and baroclinic model on a beta plane centered at 18°N latitude. It is found that the growth of synoptic scale disturbance increases with the amplitude of the meridional wind. The barotropic stability analysis at 700 hPa pressure level shows that there is a critical value ($U_{max} = 11$ m / s) of the maximum mean zonal wind below which the computed disturbance moves to the west due to the wave–wave superposition. For maximum mean zonal wind greater that 11 m / s, the westerly wind dominates and the disturbance moves to the east. In another analysis the stability of the zonally asymmetric basic flow is studied with a combined barotropic–baroclinic model where cumulus heating is included. The growth rate, intensity, horizontal scale and the westward velocity of computed disturbances reasonably agree with those of observed monsoon disturbances. The fastest growing mode has a horizontal wavelength of 2000 kms and the e–folding time is about 3 days, when the meridional amplitude of the Rossby wave is 4 m / s at 700 hPa pressure level. When cumulus heating is included in the analysis the intensity of geopotential perturbation at 700 hPa disturbance is -304 m^2 / s^2. Energy calculations show that the kinetic energy of the mean zonal flow is the main source of energy for the perturbation to grow. It is also found that the contribution of the kinetic energy of the basic Rossby wave to the growth of perturbation is more in comparison to the available potential energy.

Key words: Monsoon disturbance, Rossby wave, Combined barotropic–baroclinic stability

I. INTRODUCTION

The southwest monsoon flow is observed to be westerly in the lower troposphere and easterly in the upper troposphere. Most of the monsoon depressions are formed over north Bay of Bengal and they move in the north–west–north direction (Rao, 1976) with a speed of about 3 m / s and their doubling time is about 2–3 days (Krishnamurti et al., 1975). The wavelength of disturbance is about 2000 kms and the intensity (pressure difference) is about 4 to 8 hPa (400 to 800 m^2 / s^2 in geopotential). In order to understand the mechanism of formation of these disturbances many stability studies (Shukla, 1977, 1978; Keshavamurty et al., 1978; Mishra and Salvekar, 1980; Goswami et al., 1980; Satyan et al., 1980; Dash and Keshavamurty, 1982; Mishra and Tandon, 1983; Krishnakumar et al., 1992) of the monsoon flow have been conducted earlier. But in most of these studies only the mean zonal wind had been considered for mathematical simplicity. These stability analyses showed that the doubling time of the most unstable mode in a barotropic model was around 7 days, the horizontal wavelength was about 2000 to 3500 kms and the perturbation moved towards east at lower troposphere. But when baroclinicity and heating were included, some of these models (Mak

and Kao, 1982; Moorthi and Arakawa, 1985 and Krishna Kumar et al., 1992 and 1993) show unstable growing modes which move towards west at lower troposphere. Combined barotropic and baroclinic instability analysis with the inclusion of CISK type of heating in the model enhances the doubling time to about 2 days. The doubling time and horizontal scale of computed disturbance reasonably agree with those of observed disturbances (Krishnamurti et al., 1975) during monsoon.

Krishnamurti et al. (1984) explained that with the inclusion of orography in the model the simulated disturbances move towards west. Mishra et al. (1985) conducted a primitive equation barotropic instability analysis of the 700 hPa mean flow, similar to the earlier studies of Krishnamurti et al. (1981) and Mak and Kao (1982) concerning the monsoon onset vortex. Their most unstable mode had an e–folding time of 3 days, a wavelength of 3500 kms and a westward phase speed of 2 m / s. Goswami (1987) hypothesized that due to maximum precipitation in the western sector of the depression, the disturbances move towards west due to feedback mechanism.

The observed mean monsoon flow (Ramage and Raman, 1972) over India is zonally non–uniform and has a zonal as well as a meridional component of the wind. The magnitude of the meridional component though small may have significant effect on the characteristics of the computed disturbances. The simplest and the most plausible method of including meridional component of the wind in the basic monsoon flow is to treat the flow as the summation of the zonal mean wind and a stationary Rossby wave superimposed (Lorentz, 1972) on the former. Studies by Satyan et al. (1977), Keshavamurty et al. (1978). Dash and Keshavamurty (1982a, b and 1983) over Indian monsoon zone reveal that the amplitude of the meridional wind controls the growth rate of monsoon disturbance. Dash and Parija (1993) treated the zonal non–uniform flow as the combination of mean zonal component and a standing Rossby wave with finite amplitude along meridional direction. The quasi–geostrophic barotropic stability analysis was conducted at 700 hPa pressure level using a spectral model. The barotropic growing modes obtained in that study moved to the west as observed monsoon disturbances. This result was clearly different from those obtained in earlier barotropic models.

The essential idea of the present study is to examine whether a combined barotropic–baroclinic model with the simplest type of cumulus heating is able to explain all the characteristics of observed monsoon depressions such as the horizontal wavelength, magnitude and direction of movement, e–folding time and intensity. In Section II, a quasi–geostrophic barotropic analysis is conducted at 200 hPa pressure level. The westward movement of the fastest growing mode at 700 hPa is examined in detail and the energetics at 700 hPa and 200 hPa are computed. In Section III, a two level quasi–geostrophic combined barotropic and baroclinic spectral model is used so as to include the horizontal and vertical wind shears in the model, in the presence of cumulus heating. This model is more realistic. The characteristics of computed disturbances are examined in detail and compared to those observed during monsoon period. In Section IV, the energetics of the two level model are discussed. Section V gives concluding remarks.

II. STABILITY ANALYSIS WITH BAROTROPIC MODEL

Details of the formulation of barotropic model have been described in the earlier study by Dash and Parija (1993). For the sake of completeness, basic features of the model are briefly described here. In this section the stability analysis has been conducted for the upper level monsoon flow at 200 hPa in order to examine the characteristics of computed disturbances.

Emphasis has been given on the discussion of westward movement of the fastest computed disturbance at the lower level. Energetics have been computed at 200 hPa and 700 hPa levels.

1. *Formulation*

The quasi–geostrophic vorticity equation for barotropic atmosphere can be written as,

$$\left(\frac{\partial}{\partial t}\right)+u\frac{\partial}{\partial x}+v\frac{\partial}{\partial y}\Big)(\zeta+\beta y)=0 \ . \tag{1}$$

Here u and v are the zonal and meridional components of wind, ζ is the relative vorticity and $\beta=\frac{\partial f}{\partial y}$, f being the Coriolis parameter. The vorticity equation is linearized by expressing vorticity and zonal and meridional components of wind in the form,

$$X=\bar{x}+x', \tag{2}$$

where $\bar{x}$ is the basic component and x' is the perturbation. The basic flow is zonally non–uniform. Hence in the analysis the zonal and meridional components of the basic wind are expressed by,

$$\bar{u}=U(y) \tag{3}$$

and

$$\bar{v}=V_0\cos k_0 kx. \tag{4}$$

$U(y)$ represents the climatological mean July zonal wind at 80°E longitude (Fig. 1) and V_0 is the amplitude of the meridional wind. Here $k=2\pi/L_x$ and L_x is equal to 60° longitudes and $k_0=2$. Thus the wavelength of the basic stationary Rossby wave along the zonal direction is equal to 30° longitude (Dash and Keshavamurty, 1982b).

The normal mode analysis has been conducted by assuming a solution of the type,

$$\varphi'(x,y,t)=\sum_{m=-M}^{M}\sum_{n=-N}^{N}\varphi_{mn}e^{i(mkx+nly+\lambda t)} \tag{5}$$

for the geopotential perturbation.

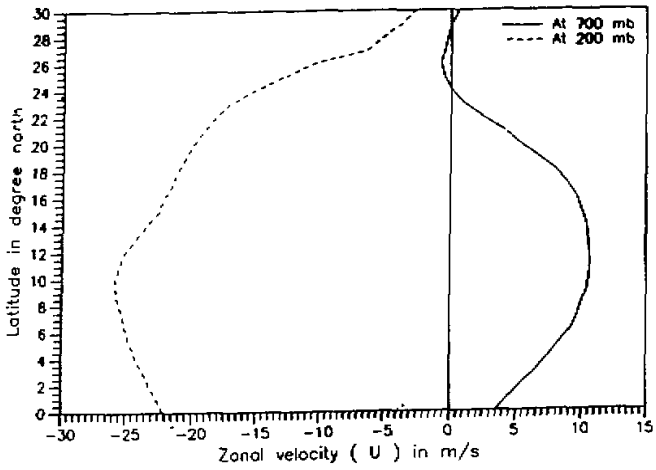

Fig. 1. Variation of zonal monsoon wind with latitude at 80°E longitude.

Here m and n are integers and $l = 2\pi / L_y$, L_y being equal to 30° latitudes. The stability analyses have been conducted over the channel 0° to 30°N latitudes with the β–plane approximation centered at 18°N. Here the values of L_x and L_y satisfy the cyclic boundary conditions imposed on the solution (5). As m and n increase in (5), perturbations of smaller scales are included in the series. Thus the solution is more general compared to earlier study by Dash and Keshavamurty (1983).

Using (2) in (1) and then subtracting the vorticity equation in the basic variables from (1), the perturbation equation will be obtained. Substituting (3) and (4), one can write the perturbation equations as

$$\left[\frac{\partial}{\partial t} + U(y)\frac{\partial}{\partial x} + V_0(\cos k_0 kx)\frac{\partial}{\partial y}\right]\zeta' - (V_0 k_0^2 k^2 \cos k_0 kx)u' + \left[\beta - \frac{\partial^2 U(y)}{\partial y^2}\right]v' = 0 \tag{6}$$

The y–dependent basic zonal wind is also expressed by Fourier series as

$$U(y) = \sum_{j=0} P_j e^{ijly} \tag{7}$$

where P_j is complex and $P_j = P_{jr} + iP_{ji}$

Calculating u', v' and ζ' from (5) and using (7) in (6) one gets the following equation after collecting the coefficients of exp $[i(mkx + nly + \lambda t)]$.

$$\begin{aligned}(\beta mk)\varphi_{mn} &+ \frac{V_0 nl}{2}\left[k_0^2 k^2 - (m-k_0)^2 k^2 - n^2 l^2\right]\varphi_{(m-k_0),n} \\ &+ \frac{V_0 nl}{2}\left[k_0^2 k^2 - (m+k_0)^2 k^2 - n^2 l^2\right]\varphi_{(m+k_0),n} \\ &+ \sum_{j=0}^{J} P_j mk\left[j^2 l^2 - m^2 k^2 - (n-j)^2 l^2\right]\varphi_{m,(n-j)} \\ &- \lambda(m^2 k^2 + n^2 l^2)\varphi_{m,n} = 0\end{aligned} \tag{8}$$

When (8) is rewritten in the matrix notation, for an eigen value problem it can be expressed as

$$(RQ^{-1} - \lambda I)\ (Q\varphi) = 0 \tag{9}$$

Here I is the unit matrix, R is a complex matrix and Q is a real matrix. The order of matrices R and Q are determined by the values of M and N in (5). Here $M = N$, hence R and Q are square matrices of order $(2N+1)$. The value of N is varied from 5 to 60 in the analysis. The eigen value λ in (5) is complex and can be expressed by

$$\lambda = \lambda_r + i\lambda_i \tag{10}$$

The real part $|\lambda_r| / 2\pi$ gives the frequency, which is multiplied by the wavelength of the perturbation to compute the phase speed. The imaginary part λ_i gives the growth rate and the disturbance will grow when $\lambda_i < 0$. The e–folding time (eft $= 1 / |\lambda_i|$) of the normal mode is computed from λ_i. $(Q.\varphi)$ in (9) is the complex eigen vector matrix from which the amplitudes φ_s are computed by inverse Fourier transformation. So the real part of the Sth eigen mode is given by,

$$R_e\,\varphi'_S(x,y,t) = |\varphi_S|\, e^{|\lambda_i|t}\cos\{\arg\varphi_S(x,y) + \lambda_r t\} \tag{11}$$

When the meridional shear is not included in the stability analysis, the constant value of U over the channel is taken to be 5.8 m / s at 700 hPa and −19.5 m / s at 200 hPa. Under this condition, the fourth term in the left hand side of equation (8) becomes equal to $-Umk[m^2k^2+n^2l^2]\varphi_{m,n}$.

2. *Characteristics of Computed Disturbances at 200 hPa*

In this stability analysis the e–folding time (eft) has been computed for the fastest growing mode. The variation of eft with M and N is shown in Fig. 2 for different values of the amplitude V_0 of the basic Rossby wave when meridional shear of the basic wind is included in the analysis. It may be noted that the observed meridional monsoon wind (Ramage and Raman 1972) at 200 hPa is northerly and hence in this study the value of V_0 is negative. In this case, as shorter waves are included the growth rate does not change very much beyond $M=N=30$, showing a tendency for saturation. For $V_0=-1$ m / s (Fig. 2) the saturated eft is about 3.9 days when $M=N=50$. When V_0 is increased from −0.5 m / s to −4 m / s, the eft of the most unstable mode decreases showing a faster growth rate. This result is similar to the growth rate in the earlier study at 700 hPa (Dash and Parija, 1993). When the basic Rossby wave is withdrawn by making its amplitude $V_0=0$, the eft of the most unstable mode increases indicating a slow growth rate. Hence the strength of V_0 controls the growth rate of perturbation at upper troposphere.

In order to examine the role of wind shear, the above computations are repeated by replacing the y–dependent zonal wind with its averaged value $U_{avg}=-19.5$ m / s over the channel. The results ar shown in Fig. 3 for different amplitudes of meridional wind. No disturbance grows with reasonable eft when V_0 is less than −8 m / s. This value of V_0 is large compared to maximum observed value (Ramage and Raman, 1972) of about 2 m / s. The eft attains its near saturated value at $M=N=55$. The saturated eft for $V_0=-8$ m / s is 3.7 days. When V_0 is increased the eft decreases as in the sheared flow, showing higher growth rate.

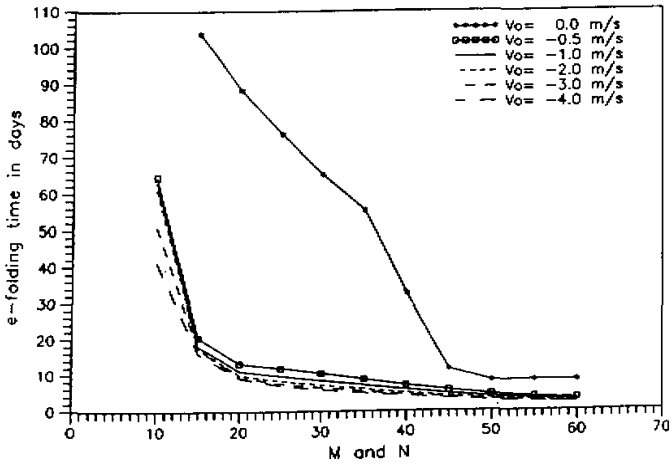

Fig. 2. Variation of e–folding time of most unstable growing barotropic mode when meridional shear is included at 200 hPa.

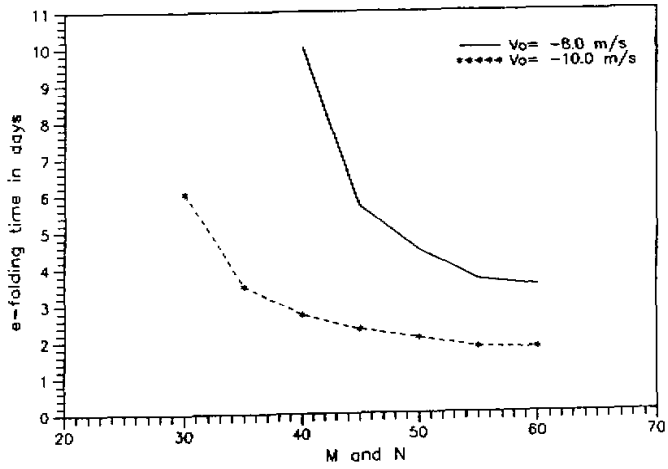

Fig. 3. Variation of e-folding time of most unstable growing barotropic mode when meridional shear is not included at 200 hPa.

The zonal phase velocities of the computed disturbances for sheared and non-sheared flow for different values of V_0 are computed and are found to be negative, indicating that the disturbances move to the west as in case of observed monsoon disturbances. The disturbances seem to be carried away by the easterly wind at upper troposphere. In case of the sheared flow the zonal phase velocity of computed disturbance is found to be about 1.7 m / s towards west for $V_0=-1$ m / s when $N=50$. For other values of V_0 there is not any significant change in the value of phase velocity.

Figure 4 shows that eft of the computed disturbance depends on its horizontal wavelength. With the inclusion of meridional wind shear in the stability analysis the horizontal

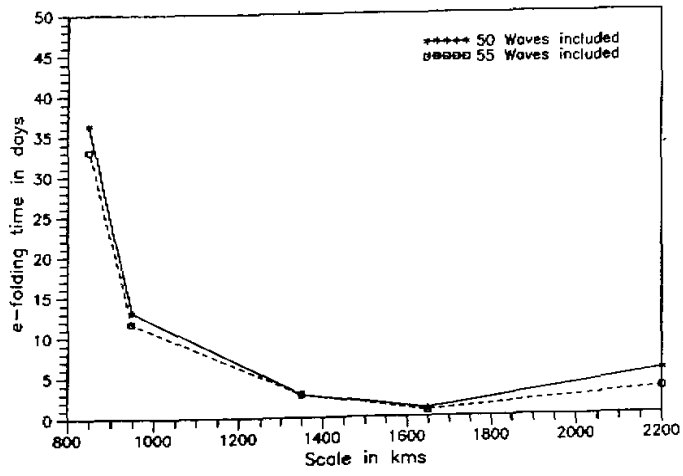

Fig. 4. Variation of e-folding time with horizontal wavelength of disturbance at 200 hPa for $V_0=-2$ m / s.

wavelength of the fastest unstable mode is found to be 1650 kms for $V_0 = -2$ m / s when $M = N = 50$ and 55. This horizontal wavelength is little less than that of the observed monsoon depressions (Krishnamurti et al., 1975) which is about 2000–2500 kms.

The horizontal structure of the most unstable mode with eft = 3.9 days for $V_0 = -1$ m / s is computed from equation (11) and is shown in Fig. 5. The horizontal scale of this disturbance is about 825 kms with the geopotential perturbation of about -2.1 m^2 / s^2 at the centre. This low is located at 18°N latitude and 84°E longitude over the east coast of India. The horizontal scale of the low is less than the observed scale (about 1000 kms) and the intensity is also very very low compared to that of the observed monsoon depressions (Rao, 1976).

3. *Westward Movement of Disturbance at* 700 hPa

The barotropic instability at 700 hPa level was analysed in another study (Dash and Parija, 1993) by using the same spectral model as discussed in Section 2.1 and the characteristics of the computed disturbances were discussed in detail. The e–folding time of the most unstable mode was about 2.4 days when $V_0 = 2$ m / s. The mode moved towards west with a phase speed of 3 m / s. The wavelength of disturbance was found to be 1650 kms. The amplitude of the low was -2.2 m^2 / s^2. In the present study some more analyses are conducted at 700 hPa with the aim of examining critically the mechanism of westward movement of monsoon depressions at the lower troposphere where the basic flow is observed to be westerly (Fig. 1). In almost all the earlier studies with barotropic model except in the primitive equation model used by Mishra et al. (1985), the computed disturbances are found to move to the east. Inclusion of cumulus heating (Krishnakumar et al., 1993) in the 3 level primitive equation model showed westward movement of disturbance. In the quasi–geostrophic model used in this study, the value of maximum zonal wind U_{max} has been varied from 10.5 m / s upto 15 m / s and also single normal mode solution is assumed in (5) instead of the summation of a

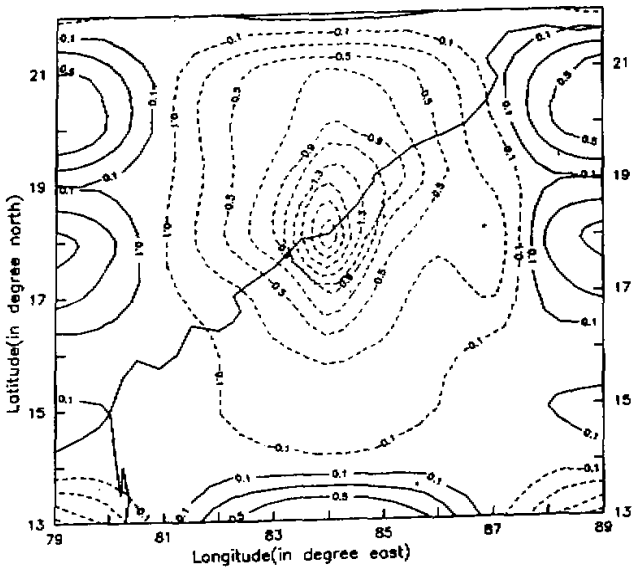

Fig. 5. Horizontal structure (geopotential) of the most unstable growing mode at 200 hPa for $V_0 = -1$ m / s, with contour interval of 0.2 m^2 / s^2.

number of waves in order to examine the dependence of the direction of movement of disturbance on the strength of the westerly and on the wave–wave superposition.

The zonal phase velocities of the computed disturbances for different values of V_0 are shown in Table 1 for $N=30$ to 50. The negative signs indicate that the computed disturbances move to the west as in case of observed monsoon disturbances. There is a tendency for saturation in the zonal phase velocity as N increases up to 50 and also the phase speed increases with V_0. The zonal phase velocity of the fastest growing computed disturbance is about −2.8 m / s for $V_0=2$ m / s at $M=N=50$ which reasonably agrees with the observed value.

Table 1. Variation of Zonal Phase Velocity of Most Unstable Mode at 700 hPa with Different Amplitudes of the Meridional Wind in the Barotropic Model

Condition	V_0 in m / s	Zonal phase velocity of most unstable eigen mode in m / s				
		$N=30$	$N=35$	$N=40$	$N=45$	$N=50$
With wind shear in the meridional direction corresponding to Fig. 1	0	−0.41	−0.47	−0.51	−0.52	−0.50
	2	−1.68	−1.92	−2.27	−2.43	−2.81
	4	−3.11	−3.46	−3.82	−4.19	−4.57
	6	−3.92	−4.35	−4.73	−5.13	−5.53
	8	−4.72	−5.20	−5.64	−6.06	−6.50
	10	−5.52	−6.04	−6.50	−7.00	−7.47

In order to identify the mechanism responsible for the westward phase speed of the computed disturbance at 700 hPa, the stability analysis was repeated by removing the summation over m in (5). The study was conducted for different values of m and the eft and phase velocities are given in Table 2. The positive signs of phase velocities in Table 2 show that all the growing modes move to the east. The disturbance with eft equal to 1.9 days moves towards east with phase speed of 8.3 m / s when $m=4$ for $V_0=2$ m / s. This result leads to the inference that superposition of waves in the solution (5) plays a dominant role in deciding the direction of movement of the disturbance. In another stability analysis the summation over m in (5) was retained and for $V_0=2$ m / s the value of basic zonal wind profile was changed so that U_{max} varies from 10.5 m / s to 15 m / s. Results (Table 3) show that for $U_{max}=10.5$ m / s and 11 m / s the preferred growing mode moves to the west but when $U_{max}>11$ m / s the mode moves to the east. This result indicates that there exists a critical value of U_{max} above which the westerly basic flow at the lower atmosphere dominates and the disturbance moves towards east. When U_{max} is less than the critical value, the wave–wave superposition dominates and the computed disturbance moves towards west.

Table 2. Characteristics of Computed Perturbation at 700 hPa When Single Wave is Considered in the Zonal Direction in the Barotropic Model for $V_0=2$ m / s

m	e–folding time in days	phase velocity (zonal in m / s)
2	6.35	7.51
3	3.08	8.22
4	1.85	8.34
5	1.29	8.38

Table 3. Characteristics of the Fastest Growing Computed Perturbation at 700 hPa for Different Zonal Wind Profiles When $V_0 = 2$ m / s

U_{max} (m / s)	e–folding time in days	phase velocity (zonal in m / s)
10.50	2.40	−2.40
11.00	2.11	−2.30
12.00	4.40	+3.10
13.00	2.54	+3.40
14.00	1.79	+3.70
15.00	1.34	+4.00

4. *Energetics of the Barotropic Unstable Mode*

In this stability analysis a basic Rossby wave of finite amplitude has been superimposed on the mean zonal wind with shear in the meridional direction. As there is no vertical wind shear, the source of energy for a perturbation to grow is the kinetic energy of the basic flow which consists of mean zonal wind $U(y)$ and the basic Rossby wave. The rate of conversion from kinetic energy of the mean zonal wind and of the basic Rossby wave to perturbation kinetic energy $C(K_b, K')$ is calculated from

$$C(K_b, K') = C(K_z, K') + C(K_w, K') \tag{12}$$

where $C(K_z, K')$ is the rate of conversion from mean zonal wind and $C(K_w, K')$ is the rate of conversion from Rossby wave.

Here

$$C(K_z, K') = -\frac{1}{g}\iiint u'v'\frac{\partial U(y)}{\partial y}\,dx\,dy\,dp \tag{13}$$

and

$$C(K_w, K') = -\frac{1}{g}\iiint u'v'\frac{\partial \bar{v}}{\partial x}\,dx\,dy\,dp \tag{14}$$

The integrations are over one wavelength of perturbation in both x and y directions and from $p = 0$ to $p = p_0$ in the vertical.

The rate of energy conversions for the most unstable mode are computed for different amplitudes of the meridional wind V_0 at 700 hPa and 200 hPa, with and without meridional shear. The results are given in Table 4. Comparison shows that $C(K_z, K')$ is greater than $C(K_w, K')$ for all the values of V_0 in the presence of meridional wind shear. It means that for the same value of V_0 increases the conversion rates $C(K_z, K')$ as well as $C(K_w, K')$ increase. For $V_0 = 2$ m / s at 700 hPa $C(K_z, K') = 2.6$ J / s and $C(K_w, K') = 0.6$ J / s. Similarly for $V_0 = -1$ m / s at 200 hPa $C(K_z, K') = 2.8$ J / s and $C(K_w, K') = 0.7$ J / s. When meridional shear of the zonal wind is not included in the stability analysis, $C(K_w, K')$ is the only source of energy and as shown in Table 4, its value increases with that of V_0. Comparing the values of $C(K_w, K')$ for $V_0 = 8$ and 10 m / s with and without meridional wind shear of zonal wind, it is interesting to note that the conversion rate from the basic wave is much less in the absence of meridional wind shear in the zonal wind. Also the conversion rate $C(K_z, K')$ from the sheared zonal wind is more in the presence of basic Rossby wave. Thus the rate of increase of kinetic energy of perturbation is more in the presence of both the meridional wind shear of the zonal wind and the stationary Rossby wave together. Presence of any one of these does not contribute significantly to the growth of the perturbation.

Table 4. Variation of Rate of Conversion of Kinetic Energy of the Basic State to That of the Most Unstable Growing Mode with Amplitude of the Meridional Velocity V_0

Condition	V_0 in m / s	Rate of conversion of kinetic energy of basic state to the perturbation in 10^{10}J / s			Level
		$C(K_Z,K')$	$C(K_W,K')$	$C(K_B,K')$	
With meridional wind shear	0	0.803	0.000	0.803	700 hPa
	2	2.564	0.554	3.118	
	4	5.421	1.031	6.453	
	6	5.450	1.233	6.683	
	8	5.516	1.865	7.381	
	10	5.440	3.208	8.649	
Without meridional wind shear	8	0.000	0.593	0.593	
	10	0.000	1.154	1.154	
	12	0.000	1.242	1.242	
With meridional wind shear	0	1.036	0.000	1.036	200 hPa
	−0.5	1.023	0.473	1.496	
	−1	2.788	0.719	3.507	
	−2	3.423	1.828	5.251	
	−3	5.242	2.093	7.335	
	−4	4.939	5.240	10.180	
Without meridional wind shear	−8	0.000	0.983	0.983	
	−10	0.000	1.378	1.378	
	−12	0.000	1.861	1.861	

III. COMBINED BAROTROPIC–BAROCLINIC TWO LEVEL MODEL

1. *Formulation of the Model*

The quasi–geostrophic vorticity and thermodynmaic energy equation for a baroclinic atmosphere with β–plane approximation can be written as,

$$\left(\frac{\partial}{\partial t}+u\frac{\partial}{\partial x}+v\frac{\partial}{\partial y}\right)\zeta+\beta v-f_0\frac{\partial\omega}{\partial p}=0 \tag{15}$$

and

$$\left(\frac{\partial}{\partial t}+u\frac{\partial}{\partial x}+v\frac{\partial}{\partial y}\right)\frac{\partial\varphi}{\partial p}+\sigma\omega=-\frac{R\dot{Q}}{pC_p} \tag{16}$$

where the symbols have their usual meaning. In this two level model one writes the vorticity equation (15) at levels 1 (200 hPa) and 3 (700 hPa) and the thermodynamic equation (16) at level 2 (500 hPa). It may be noted that hence forward, subscripts 1, 2 and 3 will be used to indicate variables at 200 hPa, 500 hPa and 700 hPa respectively. ω_2 is eliminated to get the potential vorticity equations at levels 1 and 3. $(\frac{\partial\omega}{\partial p})_{1,3}$ and $(\frac{\partial\varphi}{\partial p})_2$ are evaluated by finite difference approximation. Here the vertical boundary conditions used are $\omega_0=0$ at $p=0$ and $\omega_4=\omega_f$ at $p=p_0$.

Using relations (2), (3) and (4) in equations (15) and (16) with the above conditions at levels 1 and 2 and then subtracting the corresponding potential vorticity equations in basic variables, the linear perturbation potential vorticity equations at levels 1 and 3 can be written as

$$\left[\frac{\partial}{\partial t}+U_1(y)\frac{\partial}{\partial x}+V_{01}(\cos k_0 kx)\frac{\partial}{\partial y}\right]\left[\zeta'_1+\frac{S_2}{f_0}(\varphi'_3-\varphi'_1)\right]$$
$$+u'_1\left[S_2(V_{03}-V_{01})-V_{01}k_0^2k^2\right]\cos k_0 kx$$
$$+v'_1\left[\beta-\frac{\partial^2 U_1(y)}{\partial y^2}-S_2\{U_3(y)-U_1(y)\}\right]$$
$$=-\frac{R\Delta p S_2\dot{Q}'_2}{f_0 p_2 C_p} \tag{17}$$

$$\left[\frac{\partial}{\partial t}+U_3(y)\frac{\partial}{\partial x}+V_{03}(\cos k_0 kx)\frac{\partial}{\partial y}\right]\left[\zeta'_3+\frac{S_2}{f_0}(\varphi'_3-\varphi'_1)\right]$$
$$+u'_3\left[-V_{03}k_0^2k^2-S_2(V_{03}-V_{01})\right]\cos k_0 kx$$
$$+v'_3\left[\beta-\frac{\partial^2 U_3(y)}{\partial y^2}-S_2\{U_3(y)-U_1(y)\}\right]$$
$$-\frac{f_0\omega'_f}{\Delta p}=-\frac{R\Delta p S_2\dot{Q}'_2}{f_0 p_2 C_p} \tag{18}$$

Here $S_2=\dfrac{f_0^2}{\sigma_2(\Delta p)^2}$ and σ_2 is the static stability parameter. The value of σ_2 is taken as 3.7×10^{-2} $\mathrm{m^2sec^{-2}hPa^{-2}}$.

The normal mode analysis has been conducted to reduce the problem to an eigen value problem. Wave like solution (5) is assumed for the geopotential perturbation at both the levels.

The y–dependant basic zonal wind is expressed by Fourier series for levels 1 and 3 as in (7). Considering frictional dissipation (with Ekman layer friction), the vertical velocity ω'_f at the lower boundary ($p=p_0$) is due only to frictional pumping through Ekman layer (Charney and Eliassen, 1949). Thus

$$\omega'_f=-0.8\,\rho g\sqrt{K/2}f_0^{-3/2}(\sin 2\alpha_S)\nabla^2\sigma'_3 \tag{19}$$

The factor 0.8 is there due to the assumption that the geostrophic vorticity at the bottom boundary is 0.8 times its value at the level 3. Here K is the eddy diffusivity ($K=10\ \mathrm{m^2/s}$) and α_S is the angle between isobars and the surface wind ($\alpha_S=22.5°$). Now taking

$$F=0.8\frac{\rho g}{\Delta p}f_0\sqrt{K/2f_0}\,(\sin 2\alpha_S) \tag{20}$$

one can write

$$\omega'_f=-\frac{F\Delta p}{f_o^2}\nabla^2\varphi'_3 \tag{21}$$

The convective heating is specified only at the mid–tropospheric level. The rate of heating per unit mass (Charney and Eliassen, 1964) is given by

$$\dot{Q}'_2=H_f(p)C_p\left(\frac{P}{p_0}\right)^{R/C_p}\frac{\partial\theta}{\partial p}\omega'_f \tag{22}$$

In (22) $H_f(p)$ is the vertical distribution function for heating and is a measure of the rate of

precipitation of water vapour. θ is the potential temperature. According to Ogura (1964) the value of $H_f(p)$ at 500 hPa is taken to be 3.0. In order to examine the sensitivity to this parameter the analysis is done for H_f= 1.5, 3.0 and 4.0.

Calculating u',v' and ζ' from (5) and using (7), (21) and (22) one can rewrite the linear potential vorticity equations (17) and (18) at levels 1 and 3. Collecting the coefficients of exp[$i(mkx+nly+\lambda t)$ one gets the equations,

$$
\begin{aligned}
&(\beta mk)\varphi^1_{m,n} + \sum_{j=0}^{J} mk\left[\{j^2l^2 - m^2k^2 - (n-j)^2l^2\}P^1_j - S_2P^3_j\right]\varphi^1_{m,(n-j)} \\
&+\frac{1}{2}nl\left[V_{01}\left\{k_0^2k^2 - (m-k_0)^2k^2 - n^2l^2\right\} - V_{03}S_2\right]\varphi^1_{(m-k_0),n} \\
&+\frac{1}{2}nl\left[V_{01}\left\{k_0^2k^2 - (m+k_0)^2k^2 - n^2l^2\right\} - V_{03}S_2\right]\varphi^1_{(m+k_0),n} \\
&+\sum_{j=0}^{J}(mkS_2P^1_j)\varphi^3_{m,(n-j)} + \frac{1}{2}(V_{01}nlS_2)\varphi^3_{(m-k_0),n} \\
&+\frac{1}{2}(V_{01}nlS_2)\varphi^3_{(m+k_0),n} + iFH_f(P)(m^2k^2+n^2l^2)\varphi^3_{m,n} \\
&-\lambda\left[(m^2k^2+n^2l^2+S_2)\varphi^1_{m,n} - S_2\varphi^3_{m,n}\right] = 0
\end{aligned}
\tag{23}
$$

and

$$
\begin{aligned}
&\sum_{j=0}^{J}(mkS_2P^3_j)\varphi^1_{m,(n-j)} + \frac{1}{2}(V_{03}nlS_2)\varphi^1_{(m-k_0),n} + \frac{1}{2}(V_{03}nlS_2)\varphi^1_{(m+k_0),n} \\
&(\beta mK)\varphi^3_{m,n} + \sum_{j=0}^{J} mk\left[\{j^2l^2 - m^2k^2 - (n-j)^2l^2\}P^3_j - S_2P^1_j\right]\varphi^3_{m,(n-j)} \\
&+\frac{1}{2}nl\left[V_{03}\left\{k_0^2k^2 - (m-k_0)^2k^2 - n^2l^2\right\} - V_{01}S_2\right]\varphi^3_{(m-k_0),n} \\
&+\frac{1}{2}nl\left[V_{03}\left\{k_0^2k^2 - (m+k_0)^2k^2 - n^2l^2\right\} - V_{01}S_2\right]\varphi^3_{(m+k_0),n} \\
&+iF[1-H_f(P)](m^2k^2+n^2l^2)\varphi^3_{m,n} \\
&-\lambda\left[(m^2k^2+n^2l^2+S_2)\varphi^3_{m,n} - S_2\varphi^1_{m,n}\right] = 0
\end{aligned}
\tag{24}
$$

Equations (23) and (24) are rewritten in matrix notation so as to reduce the problem to the form of equation (9). The order of the matrix in the two level model is 2(2N+1). The structure of the most unstable growing mode at levels 1 and 3 can be computed using equation (11) at both the levels.

2. *Characteristics of Computed Disturbances*

In this study the climatological July mean zonal wind along 80°E longitude over Indian latitudes at 200 hPa and 700 hPa (Fig. 1) pressure levels are used as the basic mean zonal wind. As in the case of barotropic model, the stability analysis is conducted from 0° to 30°N latitude over India with a β–plane approximation centered at 18°N latitude. The stability analysis has been conducted with different values of meridional wind V_{01} at 200 hPa and V_{03} at 700 hPa to examine its role in the instability. In order to examine the role of cumulus heating, the combined barotropic–baroclinic two level model has been used with simple cumulus heating (H_f = 1.5,3.0,4.0) and without heating (H_f=0).

The e–folding time (eft) has been computed for the most unstable growing mode. Here

the perturbations at 200 hPa grow steadily when shorter waves are included but the growth rate does not change very much beyond $N=30$ showing a tendency for saturation with and without cumulus heating. The variation of eft of the most unstable upper growing mode with M and N is shown in Fig. 6 for different values of the amplitude of basic Rossby wave (V_{01} and V_{03}) for $H_f=1.5$. The saturated eft of the most unstable upper growing mode is about 3 days (Fig. 6) as in case of observed monsoon disturbances (Krishnamurti et al., 1975) when $N=30$ for $V_{01}=-1$ m / s and $V_{03}=4$ m / s. From Fig. 6 it is evident that eft of the most unstable upper growing mode decreases when amplitudes V_{01} and V_{03} increase at levels 1 and 3 respectively, showing a higher growth rate as in an earlier study by Dash and Keshavamurty (1982). So the amplitude of the basic Rossby wave controls the growth rate of upper tropospheric mode. There is no appreciable change of growth rate of upper tropospheric mode. There is no appreciable change of growth rate (Table 5) of the upper tropospheric mode when cumulus heating is withdrawn $H_f=0$ or introduced ($H_f=3.0$ and 4.0). Hence cumulus heating has negligible effect on the growth rate of the upper tropospheric mode. The negative sign of phase velocity (C_x) shows that the most unstable upper growing mode moves to the west (Table 5) as observed in case of monsoon disturbances. The zonal phase speed of the most unstable growing mode is about 1.1 m / s towards west for $H_f=1.5$ when $N=30$ for $V_{01}=-1$ m / s and $V_{03}=4$ m / s.

Table 5. Characteristics of the Most Unstable Upper (at 200 hPa) Growing Mode in the Two Level Model for $N=30$

Vertical heating co–eff.	$V_{01}=-0.5$ m / s $V_{03}=2$ m / s		$V_{01}=-1.0$ m / s $V_{03}=4$ m / s		$V_{01}=-1.5$ m / s $V_{03}=6$ m / s		$V_{01}=-2$ m / s $V_{03}=8$ m / s	
	Eft in Days	C_x in m / s	Eft in Days	C_x in m / s	Eft in Days	C_x in m / s	Eft in Days	C_x in m / s
$H_f=0$	3.08	−0.87	3.00	−1.16	1.50	−1.60	1.00	−1.87
$H_f=1.5$	3.17	−1.13	3.08	−1.10	1.52	−1.54	0.98	−1.50
$H_f=3.0$	3.18	−1.10	3.56	−1.07	1.52	−1.44	0.99	−1.43
$H_f=4.0$	3.22	−1.11	3.60	−1.10	1.51	−1.42	0.99	−1.42

The growth rate of perturbations at 700 hPa shows tendency for saturation at $N=45$. The results are given in Table 6. It is evident that eft of the most unstable lower growing mode decreases when amplitudes V_{01} and V_{03} increase at levels 1 and 3 respectively. So amplitude of the basic Rossby wave controls the growth rate of lower tropospheric mode also. The saturated eft of the most unstable lower growing mode is about 5.3 days when $N=45$ for $V_{01}=-1$ m / s and $V_{03}=4$ m / s under the condition that $H_f=1.5$. When the cumulus heating is withdrawn ($H_f=0$) the growth rate of the lower tropospheric mode decreases and the eft of the most unstable lower growing mode becomes 8.5 days. Hence the cumulus heating affects the growth rate of the lower tropospheric mode significantly. Following Ogura (1964) the value of the co–efficient of cumulus heating H_f is made equal to 3.0. The eft of the most unstable lower growing mode becomes equal to 3 days as observed in case of monsoon disturbances. Further increasing the value of H_f to 4.0 the eft becomes 1.7 days. In all these cases the lower tropospheric modes move towards west, when $V_{01}=-1$ m / s and $V_{03}=4$ m / s the westward phase speed (C_x) of the growing lower tropospheric mode is 1.3 m / s, 1.4 m / s, 1.5 m / s and 3.2 m / s for $H_f=0$, 1.5, 3.0 and 4.0 respectively. Thus the enhancement of cumulus heating increases the westward phase speed and the growth rate of the most unstable lower growing mode.

The structure of the most unstable growing modes are computed from Equation 11. Results show that some growing modes are predominantly lower tropospheric and some are

mainly upper tropospheric. The dominant lower tropospheric modes have maximum intensity at 700 hPa and less intensity at 200 hPa and the reverse is true for the dominant upper tropospheric modes. The horizontal structures of the most unstable upper growing mode at the two levels are shown in Figs. 7 and 8. Fig. 7 shows the horizontal structure at 200 hPa of the upper growing mode with eft = 3.5 days (Table 5) for $V_{01} = -1$ m / s and $V_{03} = -4$ m / s. The horizontal scale of disturbance is about 1000 kms which corresponds to a wavelength of 2000 kms. The amplitude of the maximum geo–potential perturbation of the low is about -44 m^2 / s^2 and its centre is located at about 20°N latitude and 88°E longitude over the Bay of Bengal. Fig. 8 shows the structure at 700 hPa of the upper growing mode with eft = 3.5 days (Table 5) for $V_{01} = -1$ m / s and $V_{03} = 4$ m / s. The horizontal wavelength is 2000 km and the amplitude of the maximum geo–potential perturbation of the low is about -36 m^2 / s^2. Its centre is located at about the same place as in the case of 200 hPa. The horizontal structures of the lower growing mode are shown in Figs. 9 & 10. Fig. 9 shows the structure at 200 hPa of the lower growing mode with eft = 3 days (Table 6) for $V_{01} = -1$ m / s and $V_{03} = 4$ m / s. As in case of upper growing mode the horizontal scale of disturbance is about 1000 kms which corresponds to a wavelength of 2000 kms. The amplitude of the maximum geopotential perturbation of the low is about -108 m^2 / s^2 and its centre is located at about 20°N latitude and 91°E longitude over the head Bay of Bengal. Fig. 10 shows the horizontal structure at 700 hPa of the lower growing mode with eft = 3 days (Table 6) for $V_{01} = -1$ m / s and $V_{03} = 4$ m / s. The horizontal wavelength of disturbance is same as in the case of 200 hPa. The amplitude of the maximum geopotential perturbation of the low is about -304 m^2 / s^2 and is seen at 20°N latitude and 92°E longitude over the head Bay of Bengal where most of the depressions are observed. The intensity of the disturbance at 700 hPa for the lower tropospheric growing mode agrees well with that of observed monsoon depression. It may be noted that 300 m^2 / s^2 geopotential is equivalent to 3 hPa pressure drop.

Table 6. Characteristics of the Most Unstable Upper (at 700 hPa) Growing Mode in the Two Level Model for $N = 45$

Vertical heating co–eff.	$V_{01} = -0.5$ m / s, $V_{03} = 2$ m / s		$V_{01} = -1.0$ m / s, $V_{03} = 4$ m / s		$V_{01} = -1.5$ m / s, $V_{03} = 6$ m / s		$V_{01} = -2$ m / s, $V_{03} = 8$ m / s	
	Eft in Days	C_x in m / s	Eft in Days	C_x in m / s	Eft in Days	C_x in m / s	Eft in Days	C_x in m / s
$H_f = 0$	9.28	−1.30	8.49	−1.32	5.25	−1.51	3.29	−1.60
$H_f = 1.5$	6.66	−1.40	5.33	−1.40	3.02	−1.55	1.42	−1.70
$H_f = 3.0$	3.51	−1.42	3.06	−1.49	1.32	−1.89	0.99	−3.07
$H_f = 4.0$	1.97	−3.00	1.67	−3.24	1.00	−3.63	0.90	−5.70

IV. ENERGETICS OF THE TWO LEVEL MODEL

In this analysis the sources of energy for the growth of perturbation are the available potential energy and the kinetic energy of the mean zonal flow and the basic Rossby wave and also the cumulus heating. The rate of energy conversions for each case are calculated to examine the dominant source of energy.

The rate of conversion of kinetic energy of the basic mean zonal wind to perturbation kinetic energy and the rate of conversion of kinetic energy of the basic Rossby wave to perturbation kinetic energy, are given by expressions (13) and (14) respectively.

The rate of conversion of available potential energy of mean zonal wind to perturbation energy is

$$C(A_Z, A') = -\frac{1}{g\sigma}\iiint v'\alpha'\frac{\partial\bar{\alpha}}{\partial y}\,dx\,dy\,dp \tag{25}$$

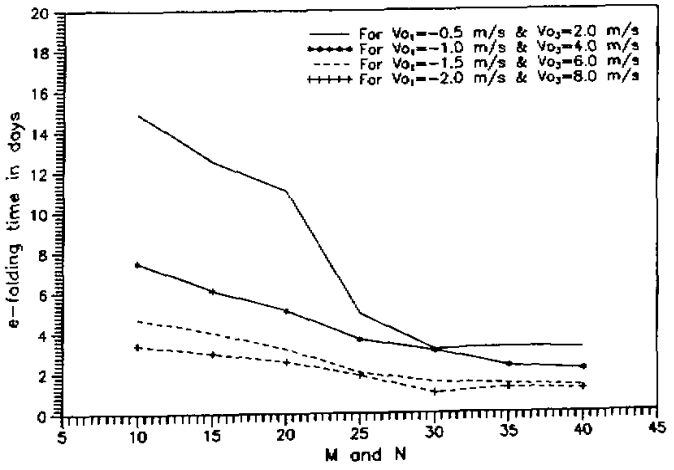

Fig. 6. Variation of e-folding time of most unstable growing upper mode of the two level model for $H_f = 1.5$.

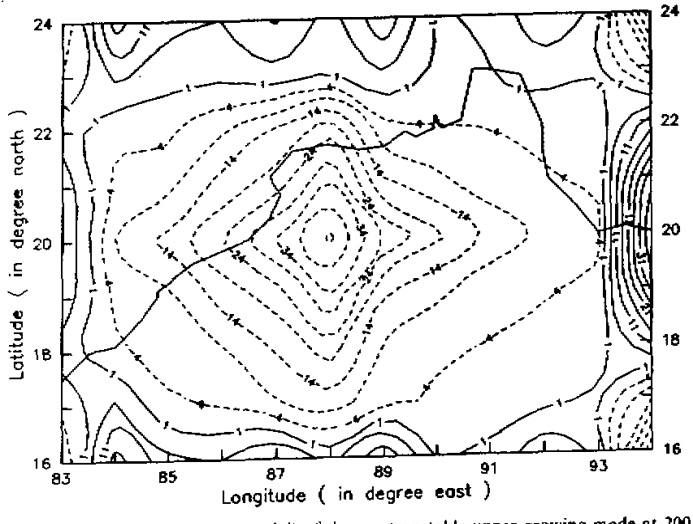

Fig. 7. Horizontal structure (geopotential) of the most unstable upper growing mode at 200 hPa for $V_{01} = -1$ m / s and $V_{03} = 4$ m / s when $H_f = 3$, with contour interval of 5 m^2 / s^2.

Similarly the rate of conversion of available potential energy of the basic wave to perturbation energy is,

$$C(A_W, A') = -\frac{1}{g\sigma}\iiint u'\alpha'\frac{\partial\bar{\alpha}}{\partial x}\,dx\,dy\,dp \tag{26}$$

The rate of conversion of heat energy to the perturbation energy is given by the following relation.

$$C(A_H, A') = \frac{1}{g\sigma}\iiint \frac{R\dot{Q}'_2}{pC_p}\alpha' dx\,dy\,dp \tag{27}$$

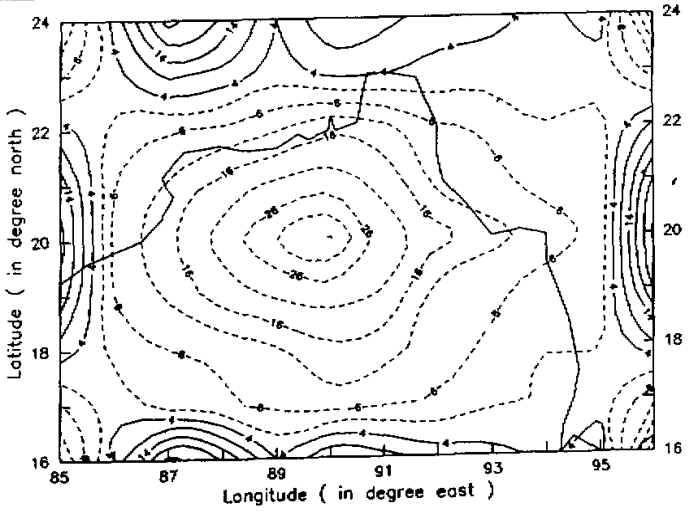

Fig. 8. Horizontal structure (geopotential) of the most unstable upper growing mode at 700 hPa for $V_{01}=-1$ m / s and $V_{03}=4$ m / s when $H_f=3$, with contour interval of 5 m^2/s^2

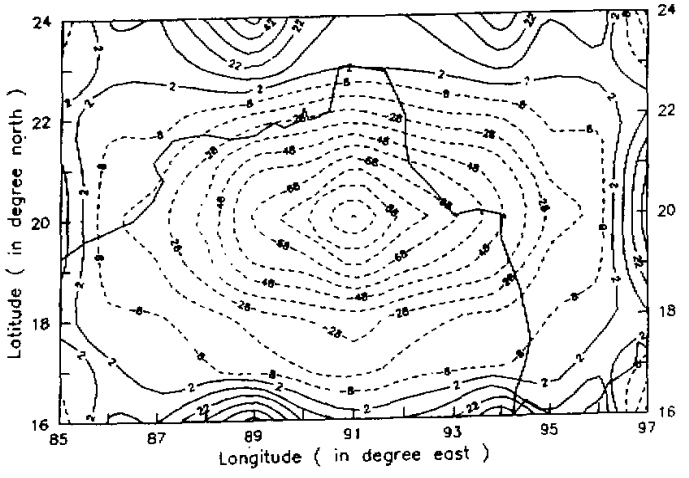

Fig. 9. Horizontal structure (geopotential) of the most unstable upper growing mode at 200 hPa for $V_{01}=-1$ m / s and $V_{03}=4$ m / s when $H_f=3$, with contour interval of 10 m^2/s^2.

The terms on the right hand side of relations (13), (14), (25), (26) and (27) can be evaluated to get the conversions. In the above equations the integrations are over the domain of one wavelength of perturbation both along x and y directions and over the depth of the atmosphere.

The total rate of change of kinetic energy from the basic state to the perturbation is

$$C(K_B,K')=C(K_Z,K')+C(K_W,K') \tag{28}$$

and the total rate of change of available potential energy from the basic state to the perturbation is

$$C(A_B,A')=C(A_Z,A')+C(A_W,A') \tag{29}$$

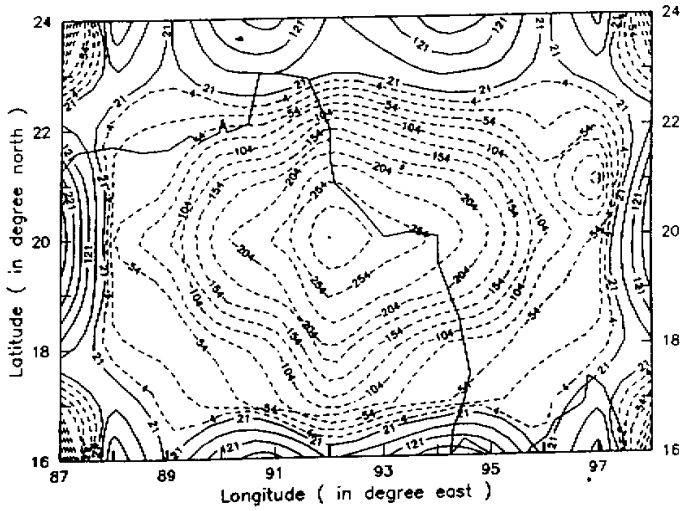

Fig. 10. Horizontal structure (geopotential) of the most unstable upper growing mode at 700 hPa for $V_{01}=-1$ m / s and $V_{03}=4$ m / s when $H_f=3$, with contour interval of 25 m^2/s^2.

The rates of conversion of energy from the basic state to the perturbation are given in Tables 7, 8 and 9 for different amplitudes of the Rossby wave. It is clear from the tables that the energy of perturbation increases with the increase of the amplitude of the Rossby wave. These results indicate that the amplitude of the Rossby wave affects the energy conversions from basic state to the perturbation as found in barotropic model. The contribution of zonal wind to the kinetic energy conversion is much more than the contribution of the basic Rossby wave. From Table 7 one gets the ratio, $C(K_Z,K')/C(K_W,K')\approx 53$ when $V_{01}=-1$ m / s, and $V_{03}=4$ m / s and $H_f=0$. In the presence of heating $H_f=3$, this ratio reduces to 16.

Table 7. Variation of Rate of Conversion of Kinetic Energy of Basic State to Perturbation Energy

Condition	V_{01} in m / s	V_{03} in m / s	$C(K_B, K')$ in 10^{10} J / s		
			$C(K_Z, K')$	$C(K_W, K')$	Total
$H_f=0$	−0.5	2	7.07	0.05	7.12
Upper	−1.0	4	11.70	0.22	11.92
growing	−1.5	6	14.80	0.73	15.53
mode	−2.0	8	35.30	3.08	38.38
$H_f=3.0$	−0.5	2	6.47	0.05	6.52
Upper	−1.0	4	8.41	0.17	8.58
growing	−1.5	6	12.03	0.24	12.27
mode	−2.0	8	23.30	0.35	23.65
$H_f=3.0$	−0.5	2	3.94	0.45	4.39
Lower	−1.0	4	7.88	0.50	8.38
growing	−1.5	6	8.26	0.55	8.81
mode	−2.0	8	9.17	0.62	9.79

From Table 8, it is seen that the rate of conversion of available potential energy of the basic state to perturbation of the upper growing mode increases with the inclusion of cumulus heating. As in case of conversion of kinetic energy (Table 7) the rate of conversion from avail-

able potential energy is less for the lower growing mode compared to the upper growing mode. The contribution of zonal wind to the rate of conversion of available potential energy is more than the contribution of the basic Rossby wave. From Table 9, it is clear that more amount of heat energy is converted to perturbation energy in case of lower growing mode compared to the respective upper growing mode. From this discussion it is clear that the perturbation gets maximum energy from the kinetic energy of the basic mean zonal wind in the presence of cumulus heating.

Table 8. Variation of rate of conversion of kinetic energy of basic state to perturbation energy

Condition	V_{01} in m / s	V_{03} in m / s	$C(A_B, A')$ in 10^5 J / s		
			$C(A_Z, A')$	$C(A_W, A')$	Total
$H_f = 0$	−0.5	2	2.20	0.06	2.26
Upper	−1.0	4	2.50	1.40	3.90
growing	−1.5	6	5.10	2.70	7.80
mode	−2.0	8	9.40	7.30	16.70
$H_f = 3.0$	−0.5	2	5.10	0.30	5.40
Upper	−1.0	4	6.60	2.40	9.00
growing	−1.5	6	9.30	6.70	16.00
mode	−2.0	8	14.30	12.80	27.10
$H_f = 3.0$	−0.5	2	1.70	0.20	1.90
Lower	−1.0	4	5.80	1.50	7.30
growing	−1.5	6	6.40	3.30	9.70
mode	−2.0	8	8.20	5.20	13.40

Table 9. Variation of Rate of Change of Heat Energy to Perturbation Energy for $H_f = 3.0$

V_{01} in m / s	V_{03} in m / s	$C(A_H, A')$ in 10^{10} in J / s	
		upper growing mode	lower growing mode
−0.5	2	0.26	1.72
−1.0	4	1.99	2.47
−1.5	6	3.75	7.73
−2.0	8	5.75	17.80

V. SUMMARY AND CONCLUSIONS

A zonally asymmetric wind profile is considered for the stability analyses by superposing a Rossby wave on the mean zonal wind. Barotropic models at 200 hPa and 700 hPa levels and a combined barotropic–baroclinic two level model are developed and used for the study. The growth rate, phase speed, direction of motion, wavelength, intensity and energetics of disturbances are computed and compared to those of observed monsoon disturbances. The results show that the growth rate and phase speed of disturbances depend very much on the amplitude of the meridional wind. In the barotropic study the wind has horizontal shear both in the zonal and meridional directions. At 200 hPa for northerly meridional wind amplitude of 1 m / s, the e–folding time of the most unstable growing mode is about 3.8 days with a westward phase speed of about 1.7 m / s and horizontal wavelength of 1650 kms. The intensity of perturbed geopotential is $-2.2\ m^2 / s^2$. The e–folding time and phase speed of the most unstable perturbation are comparable to those of the observed monsoon disturbances. The phase speed of perturbation of the barotropic growing mode of 700 hPa is towards west. It is found that when the maximum value of zonal wind at lower level (U_{max}) is changed from 11 m / s to 12 m / s, the direction of motion of perturbation changes from easterly to westerly.

Hence the results of barotropic analysis indicate that there exists a critical value ($U_{max}=11$ m / s) of the monsoon mean zonal wind at the lower troposphere below which the wave–wave superposition becomes dominant and the perturbation moves to west as in most of the observed monsoon disturbances. When $U_{max}>11$ m / s, the perturbation is carried to the east by the dominant effect of westerlies.

In the two level model, the vertical wind shear is included along with the horizontal wind shear in zonal as well as in the meridional direction. The growth rate and phase speed of perturbation obtained in the two level model also depend very much on the amplitude of the Rossby wave. The fastest growing mode at both upper and lower levels moves to the west with phase speed equal to 1.1 m / s and 1.3 m / s respectively. There is no change in the growth rate and phase speed of the upper growing mode when cumulus heating is included. But the growth rate of lower growing mode increases and the e–folding time becomes 3 days when simple type of cumulus heating with vertical heating function $H_f=3$ is introduced in the model. The fastest growing mode has a phase speed of 1.5 m / s to the west. The westward phase speed increases with the increase in heating co–efficient and becomes 3.2 m / s for $H_f=4$. The horizontal wavelength of upper and lower growing modes are 1650 kms when cumulus heating is not included but it becomes 2000 kms at both the levels with the introduction of cumulus heating of co–efficient $H_f=3$. The intensity of perturbation is low at both the levels without the cumulus heating but it enhances to reasonable value when $H_f=3$. The intensity of the lower growing mode is -108 m^2 / s^2 at 200 hPa and -304 m^2 / s^2 at 700 hPa. The computations of energetics in the barotropic model and barotropic–baroclinic two level model show that the rate of conversion of kinetic energy and available potential energy of the mean zonal wind to the perturbation energy is more than those of basic Rossby wave. The kinetic energy of the basic zonal wind in the presence of cumulus heating is the main contributing factor for the growth of perturbation in the lower level. In brief this study shows that the barotropic model can explain the growth rate, phase speed and direction of motion of the monsoon disturbances reasonably well, but in order to get the right intensity and wavelength of monsoon disturbances it is essential to use combined barotropic–baroclinic model with appropriate cumulus heating.

One of the authors (NRP) whishes to thank the University Grants Commission, India for the award of teacher fellowship which enabled him to carry out the research at Indian Institute of Technology, Delhi. The authors also thank Mr. S.K. Dutta and Mr. A.K. Swain for their help in preparing the manuscript.

REFERENCES

Charney J.G. and Eliassen A. (1949), A numerical method for predicting the perturbations of the middle latitude westerlies, *Tellus*, **1:** 38–54.

Charney J.G. and Eliassen A. (1964), On the growth of hurricane depressions, *J. Atmos. Sci.*, **21:** 68–75.

Dash S.K. and Keshavamurty R.N. (1982a), Stability of mean monsoon zonal flow, *Beitr. Phys. Atmosph.*, **55:** 299–310.

Dash S.K. and Keshavamurty R.N. (1982b), Stability of a stationary Rossby wave embedded in barotropic monsoon zonal flow, *Beitr. Phys. Atmosph.*, **55:** 311–324.

Dash S.K. and Keshavamurty R.N. (1983), Stability of a stationary Rossby wave embedded in barotropic monsoon zonal flow, *Proc. Indian Acad. Sci.* (Earth Planet Sci.), **92:** 115–119.

Dash S.K. and Parija N.R. (1993), Role of zonal assymmetry of basic wind in the instability of monsoon flow, *Proc. of Tropmet 93, India Met. Soc.* (In Print).

Goswami B.N., Keshavamurty R.N. and Satyan V. (1980), Role of barotropic, baroclinic and combined barotropic–baroclinic instability for the growth of monsoon depression and mid tropospheric cyclone, *Proc. Indian Acad. Sci.* (*Earth Planet. Sci.*), **87:** 61–75.

Goswami B.N. (1987), A mechanism for the west–north–west movement of monsoon depression, *Nature* (*London*), **326:** 376–378.

Keshavamurty R.N., Satyan V. and Goswami B.N. (1978), Indian summer monsoon cyclogenesis and its variability, *Nature*, **274**: 576–578.

Krishnakumar V., Keshavamurty R.N. and Kasture S.V. (1992), Moist baroclinic instability and the growth of monsoon depression–linear and non–linear studies, *Proc. Indian Sci. (Earth Planet. Sci.)*, **101(2)**: 123–152.

Krishnakumar V., Kasture S.V. and Keshavamurty R.N. (1993), Linear and non– linear studies of the summer monsoon onset vortex, *J. Meteor. Soc., Japan*, **71**: 1–20.

Krishnamurti T.N., Kanamitsu M., Godbole R., Chang C.B., Carr F. and Chow J.H. (1975), Study of monsoon depression (I), Synoptic structure, *J. Meteor. Soc. Japan*, **62**: 613–648.

Krishnamurti T.N., Ardanuy P.A., Ramanathan Y. and Pasch R. (1981), On the onset vortex of summer monsoon, *Mon. Wea. Rev.*, **109**: 344–363.

Krishnamurti T.N., Ingles K., Cocke S., Kitade T. and Pasch R. (1984), Details of low latitude medium range numerical weather prediction using global spectral model, Part II, Effects of eorgraphy and physical initialization, *J. Meteor. Soc., Japan*, **62**: 613–648.

Lorentz E.N. (1972), Barotropic Instability of Rossby wave motion, *J. Atmos. Sci.*, **29**: 258–264.

Mak M. and Kao C.Y.J. (1982), An instability study of the onset vortex of the southwest monsoon, 1979; *Tellus*, **34**: 358–368.

Mishra S.K. and Salvekar P.S. (1980), Role of baroclinic instability in the development of monsoon disturbances, *J. Atmos. Sci.*, **37**: 383–394.

Mishra S.K. and Tandon M.K. (1983), A combined barotropic–baroclinic instability study of the upper tropospheric tropical easterly jet, *J. Atmos. Sci.*, **40**: 2708–2723.

Mishra S.K., Patwardhan M.D. and George L. (1985), A primitive equation barotropic instability study of the monsoon onset vortex 1979, *Quart. J. Roy. Meteor. Soc.*, **111**: 427–444.

Moorthi S. and Arakawa A. (1985), Baroclinic instability with Cumulus heating, *J. Atmos. Sci.*, **42**: 2007–2031.

Ogura Y. (1964), Frictionally controlled, thermally driven circulation in a circular vortex with application to tropical cyclones, *J. Atmos. Sci.*, **21**: 610– 621.

Ramage C.S. and Raman C.R.V. (1972), Meteorological atlas of the International Indian Ocean expedition, Vol 2, Upper air, N.S.F., Washington, D.C..

Rao Y.P. (1976), South–west Monsoon, India Met. Deptt.

Satyan V., Keshavamurty R.N. and Goswami B.N. (1977), The stability of the monsoon zonal flow with superposed stationary monsoon wave, Monsoon Dynamics (eds) J. Lighthill and R. Pearce (London Cambridge University Press) 403–413.

Satyan V., Keshavamurty R.N. and Goswami B.N., Dash S.K. and Sinha H.S.S. (1980), Monsoon cyclogenesis and large scale flow pattern over South Asia, *Proc. Indian Acad. Sci. (Earth Planet. Sci.)*, **89**: 277–292.

Shukla J. (1977), Barotropic–baroclinic instability of mean zonal wind during summer monsoon, *Pure Appl. Geophysics*, **115**: 1449–1462.

Shukla J. (1978), CISK–Barotropic–baroclinic instability and the growth of monsoon depressions, *J. Atmos. Sci.*, **35**: 495–508.